Multi-Factor Component Tree Loss Function: A Topology-Preserving Method for Skeleton Segmentation from Bone Scintigrams

Anh Quynh Nguyen, Jean Cousty, Yukiko Kenmochi, Shigeaki Higashiyama, Joji Kawabe, Akinobu Shimizu

Multi-Factor Component Tree Loss Function: A Topology-Preserving Method for Skeleton Segmentation from Bone Scintigrams

Anh Q. Nguyen[1], Jean Cousty[2], Yukiko Kenmochi[3], Shigeaki Higashiyama[4], Joji Kawabe[4], and Akinobu Shimizu[1]

[1] Department of Electrical Engineering and Computer Science, Graduate School of Engineering, Tokyo University of Agriculture and Technology, Tokyo, Japan
[2] LIGM, Université Gustave Eiffel, CNRS, Marne-la-Vallée, France
[3] Normandie Université, UNICAEN, ENSICAEN, CNRS, GREYC, Caen, France
[4] Graduate School of Medicine, Osaka Metropolitan University, Osaka, Japan

Abstract. Accurate skeleton segmentation of the entire anteroposterior bone scintigrams of the human body is essential for diagnosing bone metastases. However, conventional methods lack a loss design incorporating prior anatomical information, leading to segmentation failures, particularly when dealing with the irregular shapes of organs or high concentrations of positive accumulation. Cases where diagnostic support systems present anatomically abnormal findings may shatter the confidence of doctors and their reliability in these systems. In this paper, we propose a novel multi-factor component tree loss function to resolve the topological issues in segmentation failures. The proposed loss function, computed based on the component trees, comprises two factors: image maxima vanishment and reconnection. We aim to discard the false positive connected components (FPCCs) and reconnect the disconnected true positive connected components (TPCCs) for each bone. Experiments conducted on a private bone scintigrams dataset show that our proposed method outperforms state-of-the-art approaches in dice similarity coefficient (DSC) while efficiently addressing topological issues at a low computational cost. Code is available at https://github.com/MultiCTree/MultiCTree.

Keywords: Skeleton segmentation · Bone scintigrams · Component tree.

1 Introduction

Prostate and breast cancer are the two most common cancers diagnosed in men and women, respectively, often metastasizing to the bones [1]. Bone scintigraphy, a nuclear medicine procedure, is commonly used for diagnostic purposes [2]. Bone scintigraphy produces two-dimensional images called bone scintigrams, including each patient's anterior and posterior sides. In bone scintigraphy, the Bone Scan Index (BSI) is valuable for quantitatively evaluating bone metastases spread [3]. Accurate skeleton segmentation in the anteroposterior images of the whole body is required for the calculation. Shimizu et al. [4] proposed a system

for skeleton segmentation from bone scintigrams. However, many recognition failures occurred due to high concentrations of positive accumulation and irregular organ shapes. Yu et al. [5] compared three advanced CNN-based models for skeleton segmentation without prioritizing anatomical improvement or topological evaluation metrics. To integrate topological prior, Clough et al. [6] introduced a persistent homology loss function, which can be used for n-dimensional images, although generating persistent diagrams is time-consuming. Shit et al. [7] proposed a soft-clDice loss function based on a soft skeleton algorithm. It suits tubular structures like blood vessels rather than thick structures like bones. Perret et al. [8] designed a component tree loss function to reinforce or discard image maxima based on attributes. Still, it neither reconnects components nor accurately determines components to retain or discard based on the ground truths.

In this paper, we aim to improve the anatomical correctness of segmentation failures from bone scintigrams that reduce the confidence of medical professionals. Our major contribution is proposing a novel multi-factor component tree loss function to eliminate false positive connected components (FPCCs) and establish proper reconnections among disconnected true positive connected components (TPCCs). This loss function improves the reliability of skeleton segmentation methodologies, specifically addressing challenges related to anatomical aspects.

2 Method

2.1 Max-tree

A grayscale image can be represented by a component tree, which contains all necessary information about the image components and the relationship between each component at each level of the level sets [9]. In a component tree, each connected component serves as a node, and the inclusion relationships between the connected components form the edges [8].

Let $V = \{v_i\}_{i\in[1,n]}$ denote the finite nonempty set made with n image pixels. An image is represented as a vector $\mathbf{f} \in \mathbb{R}^n$, and for any $i \in [1, n]$, $\mathbf{f}_i$ is the value of pixel v_i. For any $\lambda \in \mathbb{R}$, $[\mathbf{f}]_\lambda$ is the level set of $\mathbf{f}$ of level λ: $[\mathbf{f}]_\lambda = \{v_i \in V \mid \mathbf{f}_i \geq \lambda\}$. The *set of all connected components of* $[\mathbf{f}]_\lambda$ is denoted by $\mathcal{CC}([\mathbf{f}]_\lambda)$ and, for any λ in $\mathbb{R}$, any element in $\mathcal{CC}([\mathbf{f}]_\lambda)$ is also called a *connected component of* $\mathbf{f}$. The set of all connected components of $\mathbf{f}$ is written as $\mathcal{CC}(\mathbf{f})$, so that $\mathcal{CC}(\mathbf{f}) = \bigcup_{\lambda\in\mathbb{R}}\{\mathcal{CC}([\mathbf{f}]_\lambda)\}$. The set $\mathcal{CC}(\mathbf{f})$ is finite, and if the number of connected components of $\mathbf{f}$ is m, we can write $\mathcal{CC}(\mathbf{f}) = \{C_i\}_{i\in[1,m]}$ where C_i is the i-th connected component. The *altitude* of C_i is defined by $alt(C_i) = \max\{\lambda \in \mathbb{R} \mid C_i \in \mathcal{CC}([\mathbf{f}]_\lambda)\}$. The *max-tree* $\mathrm{MT}(\mathbf{f})$ *of* $\mathbf{f}$ is a pair $(\mathrm{MT}_1, \mathrm{MT}_2)$ made of two parts: $\mathrm{MT}_1(\mathbf{f})$ represents the connected components, and $\mathrm{MT}_2(\mathbf{f})$ is the altitude vector of the components. Thus, we have $(\mathrm{MT}_1(\mathbf{f}), \mathrm{MT}_2(\mathbf{f})) = (\{C_i\}_{i\in[1,m]}, \mathbf{a})$, where the i-th element of vector $\mathbf{a}$ in $\mathbb{R}^m$ is $alt(C_i)$ [8].

Fig. 1 shows an example of a one-dimensional image and Fig. 2 shows its max-tree. In Fig. 2, orange and green-filled rectangles represent max-tree nodes including the maxima with their altitudes. The nodes are linked in a parent-child relation (highlighted with solid lines) derived from the inclusion between

the connected components. A node without a parent is called a *root*, and one without a child is a *leaf*, also called a *maximum*.

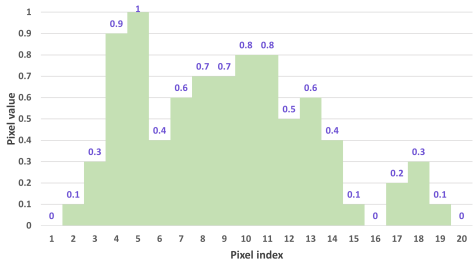

Fig. 1. One-dimensional image with pixel index and pixel value.

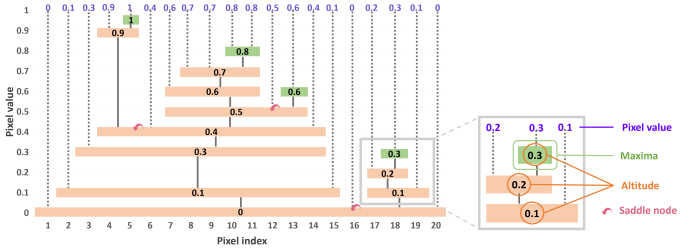

Fig. 2. Max-tree of the one-dimensional image shown in Fig. 1.

2.2 Original Component Tree Loss Function

Assuming k is the number of maxima in the hierarchy of MT($\mathbf{f}$), $\ell \in \mathbb{N}^+$ is a target maxima number, and $\mu \in \mathbb{R}$ is a constant margin to prevent selected maxima growing without limit. $\mathbf{sm} \in \mathbb{R}^k$ and $\mathbf{im} \in \mathbb{R}^k$ represent saliency and importance measures on the maxima, respectively. Importance measures rank the maxima for reinforcement or discarding while adjusting saliency measures help reinforce or discard maxima [8]. The original component tree loss function is as follows:

$$\mathcal{L}_{\text{CTree}} = \sum_{i=1}^{i \le \ell} \max(\mu - \mathbf{sm}_{\mathbf{r}_i}, 0) + \sum_{i=\ell+1}^{i \le k} \mathbf{sm}_{\mathbf{r}_i} \tag{1}$$

where $\mathbf{r} = \text{argsort}(\mathbf{im})$ is a permutation vector sorting the maxima indices of $\mathbf{f}$ in descending order of importance measure. The first term of Eq. (1) reinforces ℓ target maxima while the second term discards the others based on saliency measures. Importance measures such as *dynamics* [8] fail to distinguish TPCCs and

FPCCs while existing saliency measures cannot reconnect components. Hence, we improve the original component tree loss function by introducing and combining new saliency and importance measures into a novel loss function.

2.3 Multi-Factor Component Tree Loss Function

New Saliency "Connect" In skeleton segmentation, disconnected components within the same bone may occur. Strengthening the altitude of saddle nodes between these components can address this issue. In the max-tree (Fig. 2), a *saddle node paired to a maximum* M, denoted by $S(M)$, is the nearest ancestor of M also containing a maximum with a higher altitude than the one of M. To minimize the loss function using the saliency *dynamics* [8] (*i.e.*, $dynamics(M) = alt(M) - alt(S(M))$, one has to simultaneously decreases $alt(M)$ and increases $alt(S(M))$. However, to avoid reducing $alt(M)$ and purely establish reconnection, we propose a novel saliency measure *connect*, to reconnect these disconnected components. The saliency *connect* of M is obtained as the difference between a constant value and the altitude of the saddle node $S(M)$ paired to M. Here, let us set the constant value v to the maximum pixel value of the image as follows:

$$connect(M) = v - alt(S(M)) \tag{2}$$

In Fig. 3, the saliency *dynamics* and *connect* of each maximum are represented by blue and green double arrows, along with their corresponding values. In this case, because the maximum pixel value of the image is 1, v is set to 1.

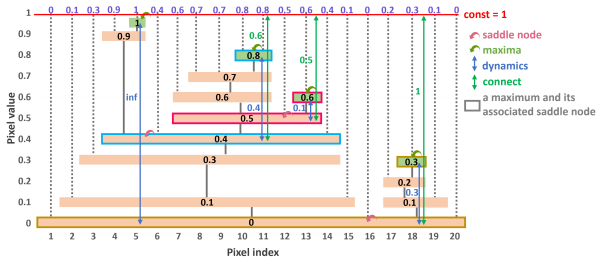

Fig. 3. Saliency measures *dynamics* and *connect*.

New Importance "Precision" The attributes of FPCCs such as *dynamics* may be higher than those of TPCCs, resulting in erroneous reconnection paths with FPCCs [8]. Therefore, we propose a novel importance measure to categorize connected components as desirable TPCCs or FPCCs. Precision measures the ratio of correctly segmented pixels to all pixels identified as ground truth by the model. A TPCC is considered desirable if it has high precision. Let G be the set

of ground truth pixels. The precision of a component C_i is defined as follows:

$$precision(C_i) = \frac{|C_i \cap G|}{|C_i|} \tag{3}$$

The importance of maxima is measured by an increasing attribute. The *extinction value* for an importance measure of a maximum M is the smallest threshold value θ at which M remains a maximum after removing all nodes with attribute values smaller than θ [8,10]. It can also be obtained as the importance measure of the saddle node $S(M)$ paired to M. Since *precision* is not increasing in the max-tree, we employed the max-rule regularization [11] on *precision* before computing the extinction value, denoted as $\mathrm{Ext}(precision(M))$. See supplementary material for more details on the calculation of the extinction value.

Combination of New Saliency and Importance Measures The new loss function integrates the proposed saliency *connect* and importance *precision*. All maxima are classified into two distinct groups: G_1 (for vanishment) and G_2 (for reconnection), as precisely defined in Table 1. Determining maxima in each group is based on the extinction value for the importance *precision* (the third column in Table 1). The *multi-factor component tree loss function* is defined as follows:

$$\mathcal{L}_{\text{multiCTree}} = \sum_{i \in G_1} \mathbf{sm_1}_i + \sum_{i \in G_2} \mathbf{sm_2}_i \tag{4}$$

where $\mathbf{sm_1} = alt$, and $\mathbf{sm_2} = connect$. It can be observed that to minimize $\mathcal{L}_{\text{multiCTree}}$, the maxima in G_1 should be eliminated by reducing their altitude, which removes FPCCs and undesirable TPCCs, while the maxima in G_2 (desirable TPCCs) should be reconnected using the saliency *connect* by increasing the altitude of their paired saddle nodes. We experimented with threshold θ values of 0.5 and 0.8 and determined that setting θ to 0.5 yields the best outcomess.

3 Experiments

3.1 Setup

Dataset Experimental bone scintigrams dataset is a DICOM-format private dataset including 1,235 cases, totaling 2,470 images from the anterior and posterior sides of female patients. Images were taken with various devices and standardized to 576×256 pixels with a 2.8×2.8 mm/pixel resolution. Segmentation targets include 13 layers for 12 anterior bones (skull, cervical vertebrae,

Table 1. Two groups of maxima: vanishment and reconnection.

Group	Saliency	Condition
G_1: Vanishment	*altitude*	$\mathrm{Ext}(precision(M_i)) < \theta$
G_2: Reconnection	*connect*	$\mathrm{Ext}(precision(M_i)) \geq \theta$

thoracic vertebrae, lumbar vertebrae, sacrum, pelvis, ribs, scapula, humerus, femur, sternum, clavicle)+background, and 14 layers for 10 posterior bones (skull, cervical vertebrae, thoracic vertebrae, lumbar vertebrae, sacrum, pelvis, ribs, scapula, humerus, femur, scapula$\cap$ribs (scapula2), scapula$\cup$scapula2 (scapula3), ribs$\cup$scapula2 (ribs2))+background. Labels were annotated by the authors in [4].

Evaluation Metrics Evaluation metrics include Dice similarity coefficient (DSC), the differences between predictions and ground truths for both (i) the number of connected components ($\Delta\#$(CCs)), and (ii) the number of TPCCs ($\Delta\#$(TPCCs)), the number of FPCCs (#(FPCCs)), and the FPCC size of each bone. Connected components are defined by 8-connectivity. These topological metrics approaching zero show better topological segmentation results. Wilcoxon signed-rank test was used for the statistical comparison, with the null hypothesis: "There is no significant difference in the performance distributions between the two methods".

Loss Function For consistent comparisons, the loss function of the model incorporating a topological loss function comprises three losses: cross-entropy loss $\mathcal{L}_{\text{CE}}$, deep supervision loss $\mathcal{L}_{\text{DSV}}$ [12] calculated based on dice loss, and a topological loss $\mathcal{L}_{\text{topology}}$. Each loss is computed independently for anterior and posterior bones and then averaged. Eq. (5) represents the total loss function. Note that the loss function of the base model is identical to Eq. (5) but without $\mathcal{L}_{\text{topology}}$.

$$\mathcal{L}_{\text{total}} = 0.5\mathcal{L}_{\text{CE}} + 0.5\mathcal{L}_{\text{DSV}} + \lambda\mathcal{L}_{\text{topology}} \tag{5}$$

3.2 Implementation Details

Three-fold cross-validation was used, with data split 4:1:1 for training, validation, and testing. Models were trained for 50 epochs on NVIDIA A100 SXM4 80 GB, Python 3.8.10, and PyTorch 1.11.10+cu115. SGD optimizer [13] had a learning rate of 0.01 and a batch size of 2. Augmentation included a horizontal flip. Loss weights were 0.01 for persistent homology loss $\mathcal{L}_{\text{PH}}$ and multi-factor component tree loss $\mathcal{L}_{\text{multiCTree}}$, and 0.1 for soft-clDice loss $\mathcal{L}_{\text{clDice}}$ and component tree loss $\mathcal{L}_{\text{CTree}}$. These weight settings optimized the performance of each model.

3.3 Experiment 1

We evaluated the computational efficiency of our method against state-of-the-art (SOTA) methods: $\mathcal{L}_{\text{PH}}$ [6] (uses a topology layer [14]), $\mathcal{L}_{\text{clDice}}$ [7], and $\mathcal{L}_{\text{CTree}}$ [8]. For computational feasibility, topological loss functions were applied solely to anterior and posterior femurs, as the persistent diagram generation process for all bones is computationally expensive. Statistical tests compared the base model TransBtrflyNet [15] with and without topological loss functions. Null hypothesis is rejected at a significance level of 0.05(*) or 0.01(*). From Table 2, all the methods improved anterior DSC but reduced posterior DSC, potentially due to conflicts between loss functions within $\mathcal{L}_{\text{total}}$. In terms of topological metrics,

except for $\mathcal{L}_{\text{PH}}$, the use of $\mathcal{L}_{\text{clDice}}$, $\mathcal{L}_{\text{CTree}}$, and $\mathcal{L}_{\text{multiCTree}}$ resulted in reductions. $\mathcal{L}_{\text{PH}}$ generated numerous #(FPCCs), leading to an increase in FPCC size, while $\mathcal{L}_{\text{clDice}}$ exhibited outstanding topological outcomes. $\mathcal{L}_{\text{multiCTree}}$ showed a superior anterior DSC and the best posterior Δ#(TPCCs) for femurs. For cases where the base model had topological issues, all topological loss functions improved results across all metrics. $\mathcal{L}_{\text{PH}}$ addressed all cases, while the others focused on cases having topological issues. See supplementary material for examples of difficult cases where images contain significant noise and numerous metastases appear on the bones. As shown in Table 3, $\mathcal{L}_{\text{PH}}$ shows the longest training time, while other methods are similar to the base model. Integrating topological loss functions does not significantly impact memory consumption. In conclusion, our methodology achieves near-optimal computational efficiency with comparable outcomes.

Table 2. Average results of femurs across 1235 cases (A: Anterior, P: Posterior; *:$p < 0.05$, **:$p < 0.01$; down arrow$^{\downarrow}$: inferiority, up arrow$^{\uparrow}$: superiority).

	Method	DSC↑	Δ#(CCs)↓	Δ#(TPCCs)↓	#(FPCCs)↓	FPCC size↓
A	Base	0.9442	0.0348	0.0178	0.0170	0.9895
	$\mathcal{L}_{\text{PH}}$	0.9449**$^{\uparrow}$	0.0672**$^{\downarrow}$	0.0211	0.0462**$^{\downarrow}$	3.0057**$^{\downarrow}$
	$\mathcal{L}_{\text{clDice}}$	0.9446	**0.0154**$^{**\uparrow}$	**0.0097**$^{*\uparrow}$	**0.0057**$^{**\uparrow}$	**0.1474**$^{**\uparrow}$
	$\mathcal{L}_{\text{CTree}}$	**0.9454**$^{**\uparrow}$	0.0251	0.0138	0.0113	0.4356
	$\mathcal{L}_{\text{multiCTree}}(\theta = 0.5)$	0.9434**$^{\uparrow}$	0.0291	0.0162	0.0130	0.5134
P	Base	**0.9422**	0.0405	0.0227	0.0178	0.6283
	$\mathcal{L}_{\text{PH}}$	0.9404**$^{\downarrow}$	0.0575*$^{\downarrow}$	0.0308	0.0267	1.4219
	$\mathcal{L}_{\text{clDice}}$	0.9414**$^{\downarrow}$	**0.0235**$^{**\uparrow}$	0.0194	**0.0040**$^{**\uparrow}$	**0.1611**$^{*\uparrow}$
	$\mathcal{L}_{\text{CTree}}$	0.9414**$^{\downarrow}$	0.0364	0.0219	0.0146	0.5085
	$\mathcal{L}_{\text{multiCTree}}(\theta = 0.5)$	0.9415**$^{\downarrow}$	0.0324	**0.0178**$^{*\uparrow}$	0.0146	0.5668

Table 3. Comparison of computational efficiency for one fold over a single epoch.

Method	Base	$\mathcal{L}_{\text{PH}}$	$\mathcal{L}_{\text{clDice}}$	$\mathcal{L}_{\text{CTree}}$	$\mathcal{L}_{\text{multiCTree}}(\theta = 0.5)$
Training time (MM:SS)	08:01	26:47	08:58	08:11	08:12
Memory (/80 GB)	37.2	37.5	37.2	37.2	37.2

3.4 Experiment 2

We applied topological loss functions to all anterior and posterior bones, with the same statistical procedure as Experiment 1. Table 4 shows the ratio of superior/inferior results to total segmentation targets (25 layers, excluding background, as defined in Section 3.1) for both anterior and posterior sides. Higher superiority ratios reflect better performance, while higher inferiority ratios show

decreased performance. $\mathcal{L}_{\text{clDice}}$ achieves the most superior results, while $\mathcal{L}_{\text{CTree}}$ has the fewest inferior results. Experiments with $\theta = 0.5$ and $\theta = 0.8$ either competed with or outperformed SOTA methods for DSC, $\Delta\#$(CCs), and $\Delta\#$(TPCCs) for both superiority and inferiority. Table 5 shows average results of all bones of all cases, where $\mathcal{L}_{\text{multiCTree}}(\theta = 0.5)$ exhibits the best results in terms of DSC, $\Delta\#$(CCs), and $\Delta\#$(TPCCs). Increasing θ to 0.8 decreased #(FPCCs) and FPCC size. Our method effectively reconnected TPCCs but concurrently generated undesirable FPCCs. $\mathcal{L}_{\text{multiCTree}}$ loss relies on the ground truths to define TPCCs and FPCCs. However, we investigated that bones such as ribs or the scapula were incorrectly labeled based on prior anatomical knowledge, resulting in an incorrect number of connected components in the ground truths. In addition, the current threshold θ is not optimal enough to eliminate FPCCs.

Table 4. The ratio of superior/inferior results to the total number of segmentation targets excluding background (S(↑): Superiority, I(↓): Inferiority).

Method	DSC		$\Delta\#$(CCs)		$\Delta\#$(TPCCs)		#(FPCCs)		FPCC size	
	S(↑)	I(↓)	S(↑)	I(↓)	S(↑)	I(↓)	S(↑)	I(↓)	S(↑)	I(↓)
$\mathcal{L}_{\text{clDice}}$	0.28	0.36	**0.24**	**0.00**	0.16	0.04	**0.32**	**0.00**	**0.12**	0.08
$\mathcal{L}_{\text{CTree}}$	0.40	0.32	0.08	**0.00**	0.04	**0.00**	0.04	**0.00**	0.08	**0.04**
$\mathcal{L}_{\text{multiCTree}}(\theta = 0.5)$	**0.72**	**0.20**	0.20	**0.00**	0.16	**0.00**	0.16	0.08	0.08	0.12
$\mathcal{L}_{\text{multiCTree}}(\theta = 0.8)$	0.48	**0.20**	0.20	**0.00**	**0.20**	**0.00**	0.12	0.08	0.04	0.08

Table 5. Average results of anterior and posterior bones across all cases.

Method	DSC↑	$\Delta\#$(CCs)↓	$\Delta\#$(TPCCs)↓	#(FPCCs)↓	FPCC size↓
Base	0.9252	0.0690	0.0646	0.0207	0.2525
$\mathcal{L}_{\text{clDice}}$	0.9262	0.0645	0.0627	**0.0126**	**0.2436**
$\mathcal{L}_{\text{CTree}}$	0.9261	0.0669	0.0626	0.0217	0.3115
$\mathcal{L}_{\text{multiCTree}}(\theta = 0.5)$	**0.9266**	**0.0578**	**0.0528**	0.0245	0.3174
$\mathcal{L}_{\text{multiCTree}}(\theta = 0.8)$	0.9262	0.0620	0.0575	0.0214	0.2880

Fig. 4 illustrates examples where $\mathcal{L}_{\text{multiCTree}}$ (fourth and fifth columns) outperformed SOTA approaches. The first row shows the capability of our method to reconnect TPCCs, while the second row highlights its ability to discard FPCCs.

4 Conclusion

This paper introduces a novel multi-factor component tree loss function, integrating saliency *connect* and importance *precision*, to improve the topological accuracy of skeleton segmentation from bone scintigrams. For future work, we will correct ground truths and optimize the threshold θ for classifying maxima.

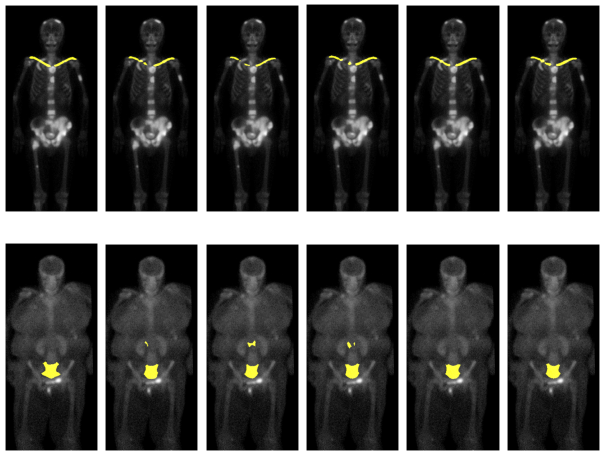

Fig. 4. Comparison of different methods applied to all bones (GT: ground truth).

Acknowledgments. This study was supported by the JSPS Sakura program (JPJSBP 120233206) and PHC Sakura program (No. 49674K).

Disclosure of Interests. Akinobu Shimizu has received research grants from Nihon Medi-Physics Co., Ltd.

References

1. Siegel, R. L., Giaquinto, A. N., Jemal, A.: Cancer statistics, 2024. CA: A Cancer Journal for Clinicians **74**(1), 8–9 (2024)
2. Donohoe, K. J., Cohen, E. J., Giammarile, F., Grady, E., Greenspan, B. S., Henkin, R. E., Millstine, J., Smith, G. T., Srinivas, S., Kauffman, J., Ahuja, S.: Appropriate Use Criteria for Bone Scintigraphy in Prostate and Breast Cancer: Summary and Excerpts. Journal of Nuclear Medicine **58**(4), 14N–17N (2017)
3. Imbriaco, M., Larson, S. M., Yeung, H. W., Mawlawi, O. R., Erdi, Y., Venkatraman, E. S., Scher, H. I.: A new parameter for measuring metastatic bone involvement by prostate cancer: the Bone Scan Index. Clinical cancer research, **4**(7), 1765–1772 (1998)
4. Shimizu, A., Wakabayashi, H., Kanamori, T., Saito, A., Nishikawa, K., Daisaki, H., Higashiyama, S., Kawabe, J.: Automated measurement of bone scan index from a whole-body bone scintigram. International journal of computer assisted radiology and surgery, **15**(3), 389–400 (2020)
5. Yu, P. N., Lai, Y. C., Chen, Y. Y., Cheng, D. C.: Skeleton Segmentation on Bone Scintigraphy for BSI Computation. Diagnostics (Basel, Switzerland), **13**(13), 2302 (2023)
6. Clough, J. R., Byrne, N., Oksuz, I., Zimmer, V. A., Schnabel, J. A., King, A. P.: A Topological Loss Function for Deep-Learning Based Image Segmentation Using Persistent Homology. IEEE transactions on pattern analysis and machine intelligence, **44**(12), 8766–8778 (2022)

7. Shit, S., Paetzold, J. C., Sekuboyina, A. K., Ezhov, I., Unger, A., Zhylka, A., Pluim, J. P., Bauer, U., Menze, B. H.: clDice - a Novel Topology-Preserving Loss Function for Tubular Structure Segmentation. In: Proceedings of the IEEE/CVF Conference on Computer Vision and Pattern Recognition (CVPR), pp. 16555–16564. IEEE Computer Society, United States (2021)
8. Perret, B., Cousty, J.: Component Tree Loss Function: Definition and Optimization. In: Baudrier, É., Naegel, B., Krähenbühl, A., Tajine, M. (eds.) Discrete Geometry and Mathematical Morphology, DGMM 2022, LNCS, vol. 13493, pp. 248–260. Springer, Cham (2022). https://doi.org/10.1007/978-3-031-19897-7_20
9. Souza, R., Tavares, L., Rittner, L. Lotufo, R.: An Overview of Max-Tree Principles, Algorithms and Applications. In: 2016 29th SIBGRAPI Conference on Graphics, Patterns and Images Tutorials (SIBGRAPI-T), pp. 15–23. Sao Paulo, Brazil (2016)
10. Vachier, C., Meyer, F.: Extinction value: a new measurement of persistence. In: IEEE Workshop on nonlinear signal and image processing, pp. 254–257. (1995)
11. Salembier, P., Oliveras, A., Garrido, L.: Antiextensive connected operators for image and sequence processing. IEEE transactions on image processing : a publication of the IEEE Signal Processing Society, **7**(4), 555–570
12. Dou, Q., Yu, L., Chen, H., Jin, Y., Yang, X., Qin, J., Heng, P. A.: 3D deeply supervised network for automated segmentation of volumetric medical images. Medical image analysis, **41**, 40–54 (2021)
13. Robbins, H., Monro, S.: A stochastic approximation method. Herbert Robbins Selected Papers, 102–109 (1985)
14. Gabrielsson, R. B., Nelson, B. J., Dwaraknath, A., Skraba, P.: A Topology Layer for Machine Learning. In: Proceedings of the Twenty Third International Conference on Artificial Intelligence and Statistics, pp. 1553–1563. (2020)
15. Nguyen, Q. A., Cousty, J., Kenmochi, Y., Higashiyama, S., Kawabe, J., Shimizu, A.: Improvement of a skeleton segmentation model of bone scintigrams with a transformer and component tree loss function. In: CARS 2023—Computer Assisted Radiology and Surgery Proceedings of the 37th International Congress and Exhibition Munich, Germany, June 20–23, 2023, Int J CARS, pp. S17–S18. (2023)